Simulation of the atmospheric methane cycle based on global monitoring data

V.N. Krupchatnikov and A.I. Krylova

Institute of Computational Mathematics and Mathematical Geophysics, Siberian Branch of the Russian Academy of Sciences, Novosibirsk

Received November 29, 2000

Simulations of the global distribution and seasonal variability of methane have been performed using a three-dimensional transport model and the NOAA/CMDL methane data for the period 1984–1987 and large-scale tropospheric fields of the OH radical. The results obtained testify to the ability of the model to reproduce the global atmospheric methane cycle. The seasonal distribution of CH_4 in the model is governed mainly by dynamic sources and the chemical sink.

Introduction

The 3D climate model of the dynamics of the atmosphere augmented by the equation of continuity for methane (CH_4) was considered in our previous study as a tracer transport model.[1] The response of the atmosphere to the CH_4 global surface distribution derived from NOAA/CMDL data on the monthly mean methane concentration near the ground surface in 1984–1987 was modeled by Boden et al.[2] on the basis of this model.

Closed contours of maximum concentrations over geographical regions of sources and adjacent areas with large gradients were obtained for the boundary layer in midlatitudes of the Northern Hemisphere by means of numerical experiments. The main result of the experiments was confirmation that the transport model makes it possible to interpolate the sparse ground-based observations at stations, most of which are far from the continental sources and sinks of methane. Since the model did not take into account atmospheric sinks of methane acting mainly in the free troposphere, it was possible to interpret the model CH_4 spatial distribution only in the boundary layer.

Results of numerical experiments simulating the global atmospheric cycle of methane in the troposphere on the basis of the NOAA/CMDL data obtained in 1984–1987 are presented in this paper. Average trends of the global cycle are revealed.

The principal mechanism of methane removal from the atmosphere – the chemical sink (reaction of methane oxidation by the hydroxyl radical in the lower and upper layers of the troposphere) is included in the tracer transport model.[1] The fraction of this channel[3] in the methane sink is ~ 0.91. Stratospheric losses of methane to generation of water vapor, and absorption of methane by soil, amount to less than 10%. As OH is the principal channel for removing not only methane but also a great number of anthropogenic admixtures from the atmosphere, it (its total content) determines their residence time in the atmosphere.

In the absence of a photochemical block in the model, by means of which it would be possible to calculate the background spatial and temporal distribution of the OH radical in the atmosphere, the monthly mean large-scale 3D fields of the OH radical obtained using the tracer photochemical model[4] were used to determine tropospheric methane losses.

Including the chemical sink mechanism in the transport model[1] makes it possible to simulate the global atmospheric methane cycle. The peculiarities of the spatial distribution of CH_4 and its annual cycle in the northern hemisphere are in qualitative agreement with analogous results[5,6] for 1984–1987.

1. Experiment

A numerical experiment simulating the global atmospheric methane cycle was performed based on the tracer transport model.[1] In addition to convective processes providing a channel for emission of methane into the atmosphere from the ground surface, photochemical losses of methane in the troposphere were included in the model. The reaction of methane oxidation by OH was considered as the principal, and in fact only, mechanism of CH_4 removal from the atmosphere

$$CH_4 + OH \rightarrow CH_3 + H_2O. \qquad (1)$$

This reaction is the stimulus of the multi-stage process of transformation of hydrocarbons.[7] As result of methane decomposition into its final products, 3.5 ozone molecules (O_3) and 0.5 OH radicals appear in place of one methane molecule disappearing in the atmosphere. The trends caused by the reaction of methane with the OH radical were calculated based on the formula

$$\frac{\partial C}{\partial t} = - LC, \qquad (2)$$

where C is the volume mixing ratio, cm^{-3}, and $L = kC_{OH}\, C_{CH_4}$ is the rate of methane loss, s^{-1}. The

0235-6880/01/06–07 468-05 $02.00

rate constant of reaction (1), according to Ref. 8, is equal to

$$k = 2.3 \cdot 10^{-12} \cdot \exp(-1700/T) \text{ cm}^3 \cdot \text{s}^{-1}.$$

The global background distribution of OH in the troposphere within the model year was obtained by interpolation of the zonal mean concentrations for four seasons, calculated based on the 3D photochemical model.[4]

The zonal mean distribution of OH used in the numerical experiment is shown in Fig. 1 as a function of the latitude and pressure for four months (January, April, July and October). The principal trends of the OH radical distribution in the atmosphere are the following:

– a decrease in the OH concentration with altitude up to the tropopause (the vertical OH profile reflects the rate of OH generation in the reaction of an oxygen atom with water vapor);

– maximum concentrations of the OH radical are observed in both hemispheres in summer at altitudes corresponding to the maximum ozone density and maximum solar insolation (600 to 800 mbar);

– in agreement with the seasonal position of the Sun, the greatest OH concentrations in January and July are observed near 30°S and 30°N, respectively.

Concentrations of OH in the troposphere undergo significant seasonal variations in the subtropics, midlatitudes and circumpolar areas. Monthly mean values of the OH concentration greater than 10^6 cm^{-3} are characteristic of the summer hemisphere from the equator to the sub-polar latitudes, while in the winter hemisphere, from 20° to the pole, they are less than 10^6 cm^{-3}.

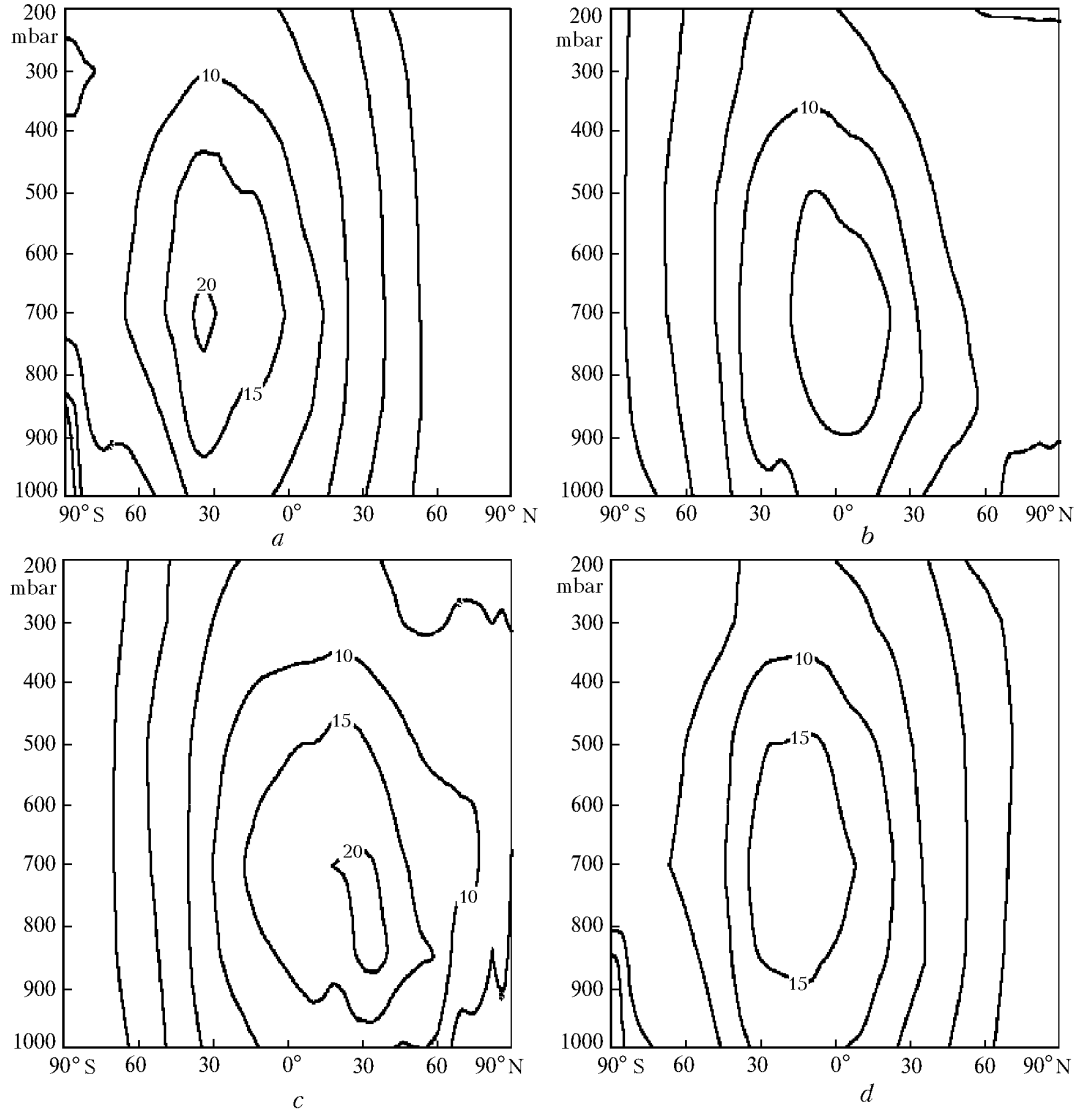

Fig. 1. Monthly mean distribution of tropospheric OH (10^5 mol · cm^{-3}) obtained using the 3D photochemical model[4] with zonal averaging for January (*a*), April (*b*), July (*c*), and October (*d*).

In the numerical experiment simulating the annual methane cycle the simulation time began on January 1 and continued for 4 years, i.e. a period sufficient to reveal stable features of atmospheric methane fields: the latitude-to-latitude gradient directed from north to south, and seasonal variations.

A globally uniform background concentration was chosen as the initial field. It was equal to zero at all levels of the model, except the Earth's surface, where the global methane distribution was obtained from a numerical analysis of the NOAA/CMDL data obtained in 1984–1987 at 19 geophysical monitoring stations.[1] To analyze the seasonal variations, the linear trend for the rate of growth equal to the global annual mean was extracted from the simulated concentrations.

2. Methane spatial distribution in the troposphere

A simulated CH_4 distribution obtained as the annual mean for a 4-year period that deviates from the global annual mean concentration at the 960-mbar level is shown in Fig. 2. It is characterized by a latitude-to-latitude gradient directed from north to south with maximum methane concentrations in the northern hemisphere.

Closed contours of the maximum concentration have been observed over North America, which are ~ 90 ppbv higher than the global annual mean values and are located over regions, where, as is well known, such continental sources of methane as supersaturated and swampy areas, and burial places of solid and liquid urban wastes are to be found.

High methane concentrations (~ 80 ppbv greater than the global annual mean values) are observed over regions of Central Europe where the sources of methane are enteritic fermentation of ruminants, supersaturated soils, and places of urban wastes.

Northeastern regions of Russia near the Arctic are characterized by a methane level ~ 70 ppbv above the global annual mean value. It is known that gas-hydrate regions are located here. Significant latitude gradients are built into the model in the north and south tropics, marking off the boundaries of the intra-tropic convergence zone. According to the simulation results at the 960-mbar level, the latitude gradient is caused mainly by atmospheric transfer, not the chemical sink. The effect of the OH radical becomes predominant in the lower and upper troposphere in the tropics.

The methane concentration near the surface in the northern hemisphere is lower over ocean regions than over the regions of continental sources by ~ 30 ppbv. A similar difference is observed over South America between the continent and the surrounding ocean.

The difference in concentrations at 550 and 960 mbar in the troposphere is shown in the upper part of Fig. 3. According to the simulation results, the concentration decreases with altitude in the northern hemisphere both over land and over the oceans, and over the continents in the southern hemisphere. One can conclude in regard to these regions that methane emission from the surface, transferred by advective and convective processes, predominates over chemical losses of methane in the formation of the vertical profile.

Closed contours of the negative difference in concentrations (the most significant difference is about 80 ppbv) provide a good indication of the location of the principal continental sources of methane on the Earth's surface. In some sense, one can consider the simulation results as a solution of the inverse problem in which the location of the methane emission source has been determined from concentrations observed over a sparse network of ground-based stations.

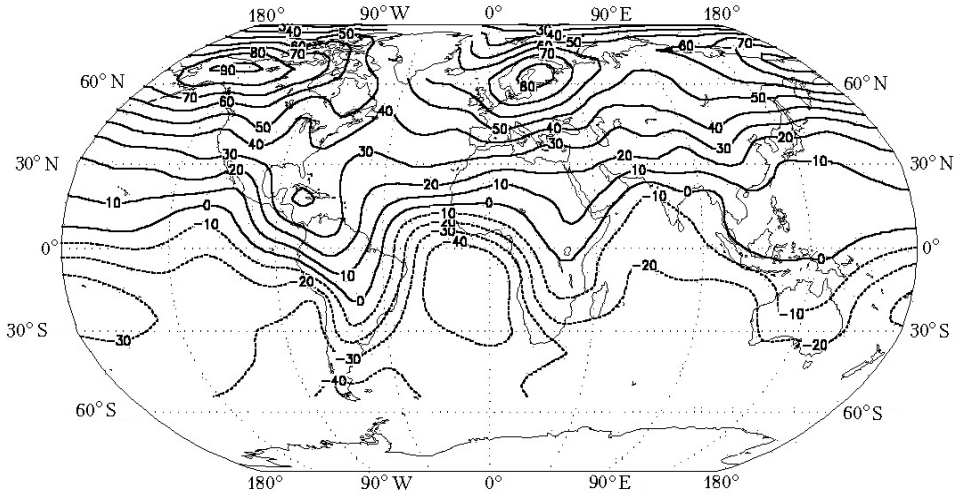

Fig. 2. Simulated annual mean distribution of the methane concentration (ppbv) at ~ 960 mbar. The concentrations are defined relative to the global mean value.

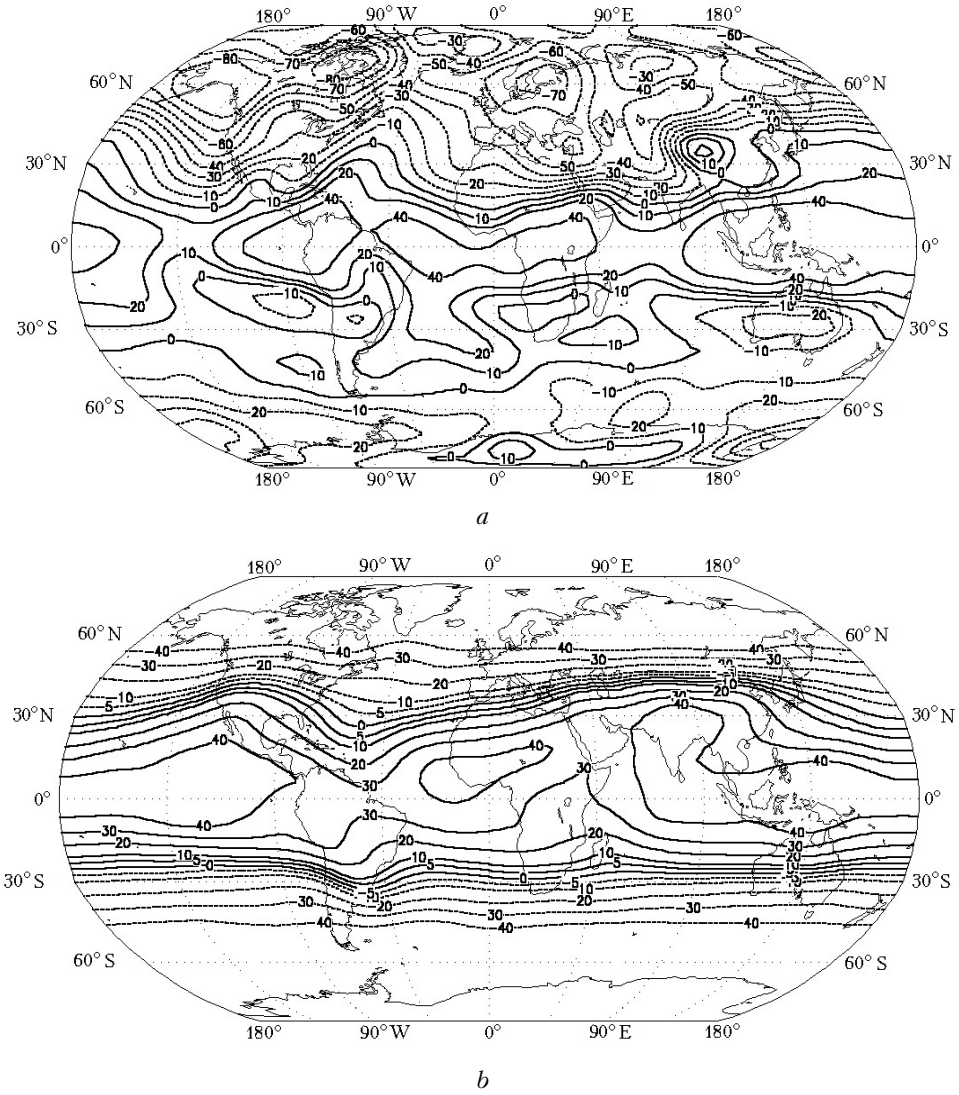

Fig. 3. Simulated annual mean distribution of the differences in the methane concentrations, ppbv, between ~ 550 and ~ 960 mbar (*a*) and between ~ 200 and ~ 550 mbar (*b*).

A positive vertical gradient is formed in the lower troposphere over oceans in the southern hemisphere. This can be explained by the fact that the signal propagating from the continental sources in the meridional direction and the signal in the latitudinal direction coming from the northern hemisphere are weak in comparison with the chemical sink. The methane concentration increases with altitude in this layer by 10–40 ppbv.

The sign of the vertical gradient in the upper troposphere, which corresponds to the pressure range from 200 to 550 mbar (lower part of Fig. 3), coincides for the most part with the sign of the gradient in the lower troposphere. However, the gradient changes sign over the continental regions of the southern hemisphere. The vertical gradient over these regions in the lower troposphere is defined by the predominance of the sources over the sink, but the situation is reversed in the upper troposphere. Methane is almost homogeneously mixed in the meridional direction above 500 mbar, and the principal mechanism forming the vertical profile is the chemical sink.

The seasonal cycle becomes apparent in the model at the 960-mbar level for the northern hemisphere as a double fall–winter maximum (Fig. 4). The emissions of peat-wetland ecosystems, which reach their maximum in September, cause the first maximum in October. This model maximum appears one month earlier than the observed data show. Oxidation by the OH radical reaches its minimum in winter. Thus, the double maximum in the seasonal behavior of methane is caused, on the one hand, by an increase of emissions in the fall, and, on the other hand, by a decrease in the sink in winter.

The minimum observed in summer in the seasonal behavior of CH_4 can be explained, in turn, by a maximum in the sink, as a consequence of the maximum concentration of the OH radical in summer. Evidently, in addition to this mechanism, one should take into account the fact that the air flows in tropics

transferred by the lower section of the Hadley cell in spring is much greater than the flows through the tropopause.

The increased methane transfer in the tropics in spring makes a definite contribution to the CH_4 minimum observed in the model at the 960-mbar level in June–July.

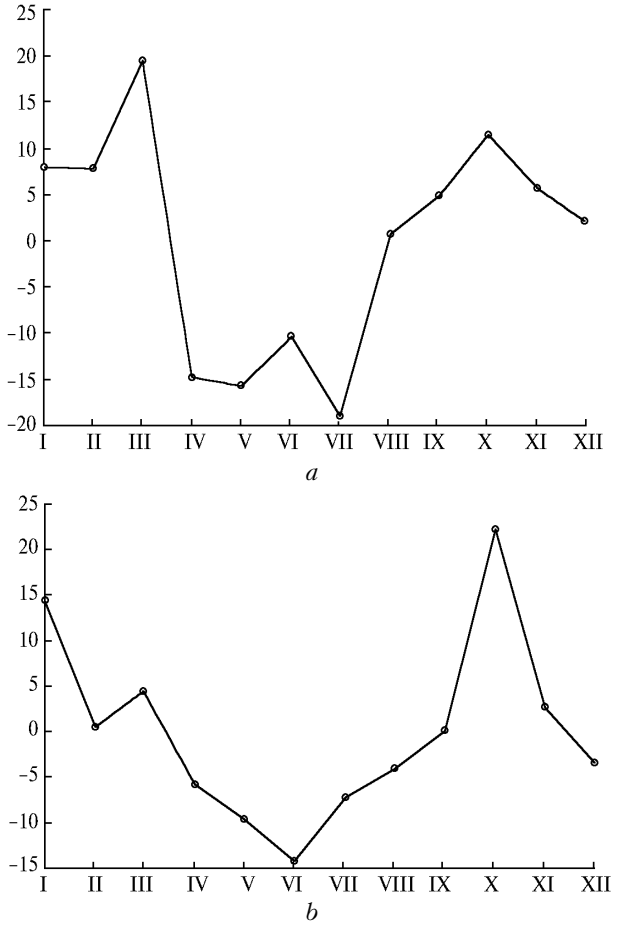

Fig. 4. Seasonal cycle of the methane concentration (ppbv) over the northern hemisphere at ~ 960 mbar at the Mould Bay station (Canada, 76°N, 119°W) (*a*) and in Belarus (53°N, 30°W) (*b*).

As was mentioned above, the CH_4 distribution in the southern hemisphere is significantly governed by the tropospheric OH distribution. By virtue of the small amplitudes of the variations in the OH concentration in comparison with the northern hemisphere, the seasonal CH_4 cycle in this hemisphere is quite weak.

Conclusion

The spatiotemporal distribution of methane in the atmosphere is obtained on the basis of a global transport model, data on the surface CH_4 concentration obtained over a 4-year period (1984–1987), and 3D fields of the OH radical. A realistic climate model of the atmosphere augmented by the continuity equation for methane[1] was used as a global transport model to study chemically reactive tracers in the atmosphere. The results obtained testify to the capability of this model to reproduce the global atmospheric cycle of methane and seasonal variations of its concentration. The simulation results are in qualitative agreement with analogous results[5,6] for 1984–1987, which underscores the adequacy of the 4-year period for revealing the principal trends in the methane distribution in the atmosphere.

Acknowledgments

This work was supported in part by the Russian Foundation for Basic Research (Grant No. 00–05–65459) and an Integration Grant of the SB RAS, No. 00–76.

References

1. V.N. Krupchatnikov and A.I. Krylova, Atmos. Oceanic Opt. **13**, Nos. 6–7, 574–579 (2000).
2. M.A. Boden, D.P. Kaiser, R.J. Sepanski, F.W. Stoss, eds., *Trends'93: A Compendium of Data on Global Change* (Tennessee, 1994), 1012 pp.
3. P.J. Crutzen, in: *Geophysiology of Amazonia*, ed. by R.E. Diskenson (Wiley, New York, 1987), pp. 107–130.
4. C.M. Spivakovsky, R. Yevich, J.A. Logan, S.C. Wofsy, and M.B. McElroy, J. Geophys. Res. D **95**, No. 11, 18441–18471 (1990).
5. I. Fung, J. John, J. Lerner, E. Matthews, M. Pratner, L.P. Steele and P.J. Fraser, J. Geophys. Res. D **96**, No. 7, 13033–13065 (1991).
6. R. Hein, P.J. Crutzen, M. Heimann, Global Biogeochem. Cycles **11**, No. 1, 43–76 (1997).
7. N.M. Bazhin, Khimiya v Interesakh Ustoichivogo Razvitiya **1**, 381–396 (1993).
8. W.B. DeMore, M.J. Molina, S.P. Sander, D.M. Golden, R.F. Hampson, M.J. Kurylo, C.J. Howard, and A.R. Ravishankara, JPL Publ., 87–91 (1987).